An estimation of annual new production and carbon fluxes in the northeast Atlantic Ocean during 2001

Camila I. Fernandez, Patrick Raimbault, Nicole Garcia, Peggy Rimmelin, Guy Caniaux

An estimation of annual new production and carbon fluxes in the northeast Atlantic Ocean during 2001

Camila Fernández I., Patrick Raimbault, Nicole Garcia, and Peggy Rimmelin

Laboratoire d'Océanographie et de Biogéochimie, UMR 6535, Centre National de Recherche Scientifique, Centre d'Océanologie de Marseille, Université de la Méditerranée, Marseille, France

Guy Caniaux

National de Recherche Météorologique, Toulouse, France

Received 22 July 2004; revised 21 March 2005; accepted 19 May 2005; published 7 July 2005.

[1] A dual $^{13}C/^{15}N$ isotopic technique was used to estimate carbon and nitrogen uptake rates during the 1-year-long Programme Océan Multidisciplinaire Méso Echelle (POMME) experiment in the northeast basin of the Atlantic Ocean (16°–22°W, 38°–45°N). Rates of primary production ranged from 2.26 μmoles L^{-1} d^{-1} in winter to maximum surface values of 7.8 μmoles L^{-1} d^{-1} during the spring season. Nitrate assimilation was intense since the beginning of winter and accounted for 3–7 mmoles m^{-2} d^{-1} in the first 80 m depth of the water column. Rates increased to 5–9 mmoles m^{-2} d^{-1} during the spring season. NO_3^- uptake rates during the late summer season were close to winter values. Ammonium assimilation activity balanced the uptake of nitrate for all seasons. The seasonal *f* ratio was close to 0.28 in winter, increased to 0.34 in spring, and, finally, decreased to 0.25 in late summer. Annual carbon uptake rates for the entire POMME area accounted for 16.9 moles C m^{-2} yr^{-1}. From this result, annual new production could be estimated to 5.7 moles C m^{-2} yr^{-1}.

Citation: Fernández I., C., P. Raimbault, N. Garcia, P. Rimmelin, and G. Caniaux (2005), An estimation of annual new production and carbon fluxes in the northeast Atlantic Ocean during 2001, *J. Geophys. Res.*, *110*, C07S13, doi:10.1029/2004JC002616.

1. Introduction

[2] The spring bloom in the North Atlantic Ocean is known as one of the most conspicuous seasonal events in the world ocean [*Ducklow and Harris*, 1993; *Donald et al.*, 2001]. Concerning its physical background, several studies have described the area between 40°N and 60°N as a transition zone between the subtropical gyre and the sub polar waters, with an average sink for atmospheric CO_2 [*Takahashi et al.*, 1995, 1997, 1999, 2002; *Louanchi and Najjar*, 2001; *Álvarez et al.*, 2003] mostly active during the spring [*Rios et al.*, 1992].

[3] According to *Dugdale and Goering* [1967], "new" production is fuelled by allochthonous N sources (mainly NO_3^-) mixed into surface waters from the deep ocean. On the other hand, "regenerated" production is fuelled by autochthonous N sources (mainly NH_4^+), derived from biological processes [*Harrison et al.*, 1987]. The fraction of primary production based on new nutrients (usually NO_3^-) is termed the *f* ratio [*Eppley and Peterson*, 1979] and, at steady state, accounts for the proportion of production available for export. New production estimates, computed in terms of carbon by using the *f* ratio and primary production, has known considerable variability [*Aufdenkampe et al.*, 2002], due to the inaccuracy in estimating *f* and NO_3^- assimilation [*Priscu and Downes*, 1985; *Ward et al.*, 1989; *Gentilhomme and Raimbault*, 1994; *Raimbault et al.*, 1999; *Diaz and Raimbault*, 2000; *Aufdenkampe et al.*, 2001].

[4] New production estimates are often obtained from, for instance, surface nitrate fields and remotely sensed sea surface temperature [*Sathyendranath et al.*, 1991; *Morin et al.*, 1993; *Henson et al.*, 2003], applied to wide areas of the ocean. They can also be inferred from models applied to specific environments [*Dugdale et al.*, 1997]. However, the robustness of such estimations has proven to be sensitive to the seasonality of physical forcing in the North Atlantic [*Henson et al.*, 2003].

[5] Concerning in situ nitrogen uptake, there have been a number of crucial findings that have led to the identification of several sources of "new nitrogen" for new production, (e.g., N_2 fixation [*Gruber and Sarmiento*, 1997]) (see review by *Lipschultz et al.* [2002]). Other than physical processes, regeneration of nitrogen occurring in situ can also represent a significant source of nutrients for the surface layer of the ocean. However, the impact of such processes is still rarely accounted as a possible overestimation factor in new production calculations. Until the last decade, nitrification, the oxidation of ammonium to nitrate mediated by nitrifying bacteria, was thought to be restricted to specific environments but it is now known that it is more widely distributed [*Zehr and Ward*, 2002]. Its role in providing regenerated nitrate in the euphotic zone has been exposed by several studies [*Ward et al.*, 1989; *Dore and Karl*, 1996] and confirmed by recent findings in the NE

0148-0227/05/2004JC002616

Atlantic, where nitrification can support 5–100% of new production [*Fernández*, 2003]. By overestimating new production, the significant part of the available nitrate that should account for regenerated rather than new production can have a significant impact in the calculations of the *f* ratio, and therefore on the fraction of biological production that is really available for export.

[6] Ammonium regeneration is another source of regenerated nitrogen to the euphotic zone. By studying ammonium isotopic dilution (recycling of unlabeled substrate) during ^{15}N incubation experiments, *Glibert et al.* [1982] and *Harrison et al.* [1987] showed that ammonium regeneration can result in significant underestimations of regenerated production; which would also bias the assessment of the *f* ratio.

[7] As our understanding of the nitrogen cycle moves on, these facts lead to a new revision of the *f* ratio and to important implications for the annual budget of the carbon and nitrogen cycles in the North Atlantic.

[8] The Programe Océan Multidisciplinaire Méso Echelle (POMME) was scheduled to provide a complete data set of physical and biogeochemical parameters with a mesoscale resolution, in the northeast Atlantic basin (16°–22°W, 38°–45°N (Figure 1)). The present work focused on the seasonal evolution of primary production and nitrogen assimilation in order to accurately estimate annual new production and carbon fixation. Our data contributed to the objectives of POMME [*Mémery et al.*, 2005], by providing a yearlong survey of the productive system in the study area. It is also a step forward in the appreciation of how varying biogeochemical and physical processes can force shifts between high and low export production, as this is a key issue to understanding the relationship between mesoscale processes, mode water formation and the future significance of the biological pump.

2. Methods

[9] Data were gathered during the first leg of three consecutive POMME cruises [*Mémery et al.*, 2005], carried out during 2001.

[10] The evolution of mesoscale features during and between surveys was simulated weekly by the SOPRANE model (based on CTD and XBT), which assimilates data coming from drifters and floats (Marvors, Provors and Surdrifts [*Le Cann et al.*, 2005]) released in the POMME area, as well as altimetry data [*Assenbaum and Reverdin*, 2005]. In parallel, CTD, XBT and XCTD data gathered during these surveys were used in order to obtain high-resolution temperature and salinity analyses, from which geostrophic current maps were derived as described by *Fernández et al.* [2005].

[11] The first cruise (POMME 1 Leg 1, 31 January–24 February 2001) was conducted during the winter season in order to describe prebloom conditions. From a total amount of 79 stations (performed on a 55.5 km grid), 29 stations were completed with production experiments (Figure 1a). The spring cruise (POMME 2 Leg 1, 23 March–13 April 2001) was performed immediately after POMME 1 and following a similar sampling strategy. From a total amount of 81 stations on the sampling grid, 22 were production stations (Figure 1b). During the late summer cruise (POMME 3 Leg 1, 25 August–12 September 2001; R/V *Thalassa*); the sampling grid included 83 standard stations and 25 production stations (Figure 1c).

2.1. Nutrients

[12] Nutrient measurements (NO_3^-, NO_2^-, and $PO4^-$) were performed at every station of the grid. For each depth level, samples were taken in 20 mL polyethylene flasks and analyzed on board immediately after sampling according to *Armstrong et al.* [1967], using a semi automatic Technicon Autonanalyser® (AAII). Ammonium concentrations (NH_4^+) were measured between the surface and 200 m depth at approximately half of the stations. The detection limits are 0.05 μmoles L^{-1}, 0.02 μmoles L^{-1}, 0.02 μmoles L^{-1} and 0.01 μmoles L^{-1} for NO_3^-, NO_2^-, PO_4^- and NH_4^+, respectively. To ensure reproducibility in nutrient measurements between cruises, a unique type of in-house standards was used from POMME 1 through POMME 3, which was regularly compared to commercial products (OSIL). Precision was also tested, through the participation in the European intercalibration exercise QUASIMEME (http://www.quasimeme.marlab.ac.uk).

2.2. Production Experiments

[13] At each production station, rates of carbon uptake (primary production), nitrate (new production) and ammonium assimilation (regenerated production) were measured by using a dual isotopic technique ^{13}C-$^{15}NO_3$ and ^{13}C-$^{15}NH_4$. In parallel, ^{13}C exclusive assimilation experiments were conducted for every profile. For this purpose, three 600 mL samples were collected before sunrise at 6 standard depths between the surface and 80 m and poured into acid-cleaned polycarbonate flasks (PC) flasks for carbon (^{13}C) and nitrogen (^{13}C-$^{15}NO_3^-$ and ^{13}C-$^{15}NH_4$) uptake experiments. Bottles were rinsed after use with 10% HCl, then with distilled water from a Milli Q ion exchange unit.

[14] Incubations were done on deck in an incubator, which consisted of six opaque boxes, each with a light screen that allowed 50%, 25%, 15%, 8%, 4% and 1% of light penetration; the incubator was maintained at sea surface temperature with pumped sea water.

[15] After 12 hours (dawn to dusk), incubations were terminated by filtration onto 25 mm precombusted Whatman® GF/F filters using a low vacuum pressure (<100 mm Hg). After filtration, filters were stored in precombusted glass tubes in a 60°C oven until mass spectrometry analysis was conducted at the laboratory using a Europa Scientific® Tracer Mass (Roboprep and ANCA MS).

2.2.1. Primary Production

[16] Carbon fixation was measured using the ^{13}C isotopic technique [*Slawyk et al.*, 1977; *Slawyk and Collos*, 1984; *Slawyk et al.*, 1984]. Carbon-13 tracer concentration was 3.6456 mg^{13}C mL^{-1}, which is equivalent to 0.5 μmoles mL^{-1}. To each sample, 0.5 ml of ^{13}C tracer was added, which roughly corresponds to 10% enrichment.

[17] Carbon assimilation (μmoles C L^{-1} d^{-1}) was obtained using equation (1):

$$\rho^{13}C = \left[\frac{(R_{POC} - R_n) * \left(\frac{POC}{12 * V_f} \right)}{R_{DIC}} \right], \quad (1)$$

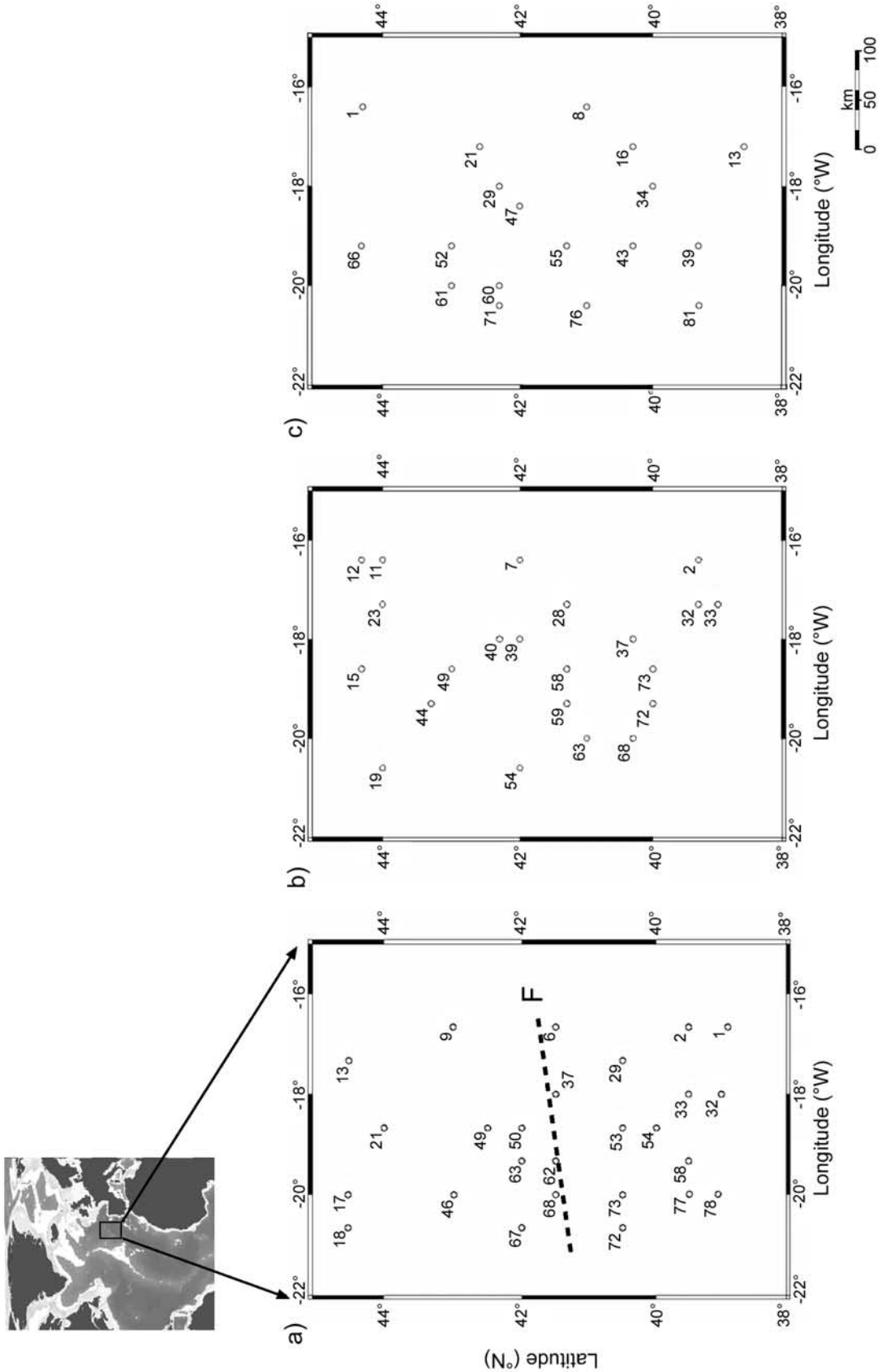

Figure 1. Map showing the location of the study area and the location of the conductivity-temperature-depth (CTD) cast where $^{15}N/^{13}C$ enrichment experiences were performed during (a) P1, (b) P2, and (c) P3. The dotted line represents the theoretical location of the hydrological front (F).

where V_f represents the volume filtered after incubation, POC represents the amount of particulate organic carbon recovered in the filter and measured by mass spectrometry (μg), and R_{POC} indicates the ^{13}C enrichment in the filter after incubation (in %), measured by mass spectrometry. The term R_n represents the average natural abundance of ^{13}C in particulate organic carbon (1.112%). The excess enrichment of the tracer after inoculation (T_0) is indicated by R_{DIC} (in %), and is calculated using equation (2):

$$R_{DIC} = \frac{\left[\left(\frac{V^{13}C * {}^{13}DIC}{V_b}\right) + DIC_i * 0.01112\right] * 100}{DIC_i + \frac{V^{13}C * {}^{13}DIC}{V_b}}, \quad (2)$$

where $V^{13}C$ indicates the volume of the ^{13}C tracer solution, added to the sample before incubation (0.5 mL). ^{13}DIC represents the concentration in ^{13}C of the added tracer (3.6456 mg ^{13}C mL^{-1}). The term 0.01112 represents the average natural abundance of ^{13}C (in absolute value). DIC_i represents the concentration of DIC in the sample, before tracer addition. This value was assumed constant (28 mg C L^{-1}). V_b is the volume in the incubation flask (in liters).

2.2.2. Nitrogen Assimilation

[18] Nitrate and ammonium uptake experiments were carried out using the dual isotopic technique, which allowed measuring carbon and nitrogen assimilation in the same sample (^{13}C-$^{15}NO_3$; ^{13}C-$^{15}NH_4$). Therefore two nitrogen uptake experiment flasks ($^{15}NO_3$ and $^{15}NH_4$) were also inoculated with ^{13}C, using the same ^{13}C tracer concentrations described in section 2.2.1. This was used to test the absence of interference of primary production caused by a possible stimulation due to $^{15}NO_3$ or $^{15}NH_4$ additions.

[19] For nitrate and ammonium uptake measurements, samples were collected using the same method described in section 2.2.1. Immediately after sampling, ambient NO_3^-, NO_2^- and NH_4^+ concentrations were measured directly from the PC flasks, according to *Armstrong et al.* [1967]. Nitrogen 15 tracer additions as $K^{15}NO_3$ or $^{15}NH_4Cl$ (99% at ^{15}N) were usually 10–20% of the ambient concentration. In nutrient impoverished waters during the late summer season, minimal additions of ^{15}N resulted in substrate enrichments of 50–100% (~43 nmoles L^{-1} $^{15}NO_3$; ~87 nmoles L^{-1} $^{15}NH_4$). In such case, ^{15}N additions are likely to perturb the phytoplanktonic environment leading to potential productivity measures rather than real uptake [*Allen et al.*, 1996; *Harrison et al.*, 1996; *Raimbault et al.*, 1999]. The initial NO_3^- and NH_4^+ concentrations (T_0 values) were usually verified after tracer addition. As described in section 2.2, samples were incubated on deck from sunrise to sunset.

[20] Following incubation, concentrations of NO_3^- and NH_4^+ were measured directly from the PC flask and samples were filtered thereafter on Whatman GF/F filters. Subsequent to filtration, filters were dried at 60°C and stored in the oven until laboratory analysis. These filters were used to determine the final ^{15}N enrichment in the particulate organic nitrogen (PON) pool, which exclude bacterial uptake of NH_4^+ and NO_3^-. At the same time, filtrates were recovered in Duran Schott flask and poisoned with 1 mL $HgCl_2$ (6 g L^{-1}). These filtrates were used to measure the final ^{15}N enrichment in the dissolved inorganic nitrogen (DIN) pool, as outlined by *Slawyk and Raimbault* [1995]. In this procedure, all forms of DIN were removed from the sample as ammonium sulphate, by successive diffusion and reduction processes. The ammonium sulphate was later collected on glass fiber filters that were analyzed by mass spectrometry. The measurement of the isotopic enrichment in the DIN pool provides a check on the isotope dilution of the ^{15}N tracer due to DIN regeneration and thus corrects (for underestimation of) DIN uptake rates. The transport rate of ^{15}N-labelled DIN from the DIN pool to the PON pool, i.e., the net DIN uptake (ρ^{net}_{DIN} in nmoles L^{-1} d^{-1}) was computed, according to *Dugdale and Wilkerson* [1986], from equation (3):

$$\rho^{net}_{DIN} = \frac{R_{PON}}{R_{DIN} \times T} \times [PON], \quad (3)$$

where R_{PON} and R_{DIN} represent the ^{15}N atom% excess enrichment in the PON and DIN pools respectively, [PON] represents the final PON concentration and T represents the incubation period (in hours). As mentioned before, to correct ammonium uptake rates for isotopic dilution, we made R_{DIN} in equation (3) equal to the mean value between initial and final R_{NH_4}.

[21] Nitrate uptake rates were corrected for ammonium oxidation rates (hereafter referred as nitrification). Nitrification rates can be obtained from filtrates enriched in $^{15}NH_4$, through the estimation of the amount of nitrate formed during incubation [*Raimbault et al.*, 1999; *Diaz and Raimbault*, 2000]. Consequently, for NH_4 filtrates, an intermediate diffusion step was added in order to obtain the ^{15}N abundance (NO_3^- and NO_2^-) pool, i.e., to estimate nitrification (here, oxidation steps from NH_4^+ to NO_2^-, and from NO_2^- to NO_3^-). Nitrification rates (ρ_{NIT} in nmoles L^{-1} d^{-1}) were computed by using equation (4) [*Raimbault et al.*, 1999]:

$$\rho_{NIT} = \frac{R_{NO_3}}{R_{NH_4} \times T} \times [NO_3], \quad (4)$$

where R_{NO_3} is the ^{15}N atom% excess enrichment in the NO_3^- (+ NO_2^-) pool, R_{NH_4} is the mean ^{15}N atom% excess enrichment of the NH_4^+ pool, and $[NO_3]$ is the final NO_3^- concentration in the filtrate. T represents the incubation period, in hours. The rates of $^{15}NH_4$ oxidation to $^{15}NO_3$ by nitrification were then subtracted from nitrate uptake rates when computing new production (new nitrate assimilation).

2.2.3. Estimating the *f* Ratio

[22] The definition of the *f* ratio given by *Eppley and Peterson* [1979] is illustrated by equation (5), where ρNO_3^- accounts for new production as "new" nitrate assimilation and $[\rho(NO_3^-) + \rho(NH_4^+)]$ represents the uptake of total nitrogen. In this definition, in situ regenerated nitrate is not included as a substrate for total nitrogen production. Moreover, the definition of new production is based on the assimilation of nitrate, without any distinction about its origin, whether it comes from nitrification or vertical mixing. However, nitrification as a source of nitrate can induce an overestimation of new production, by adding to the nitrate pool, some NO_3^- coming from what is, actually, regenerated production. Hence for *f* ratio calculation in this

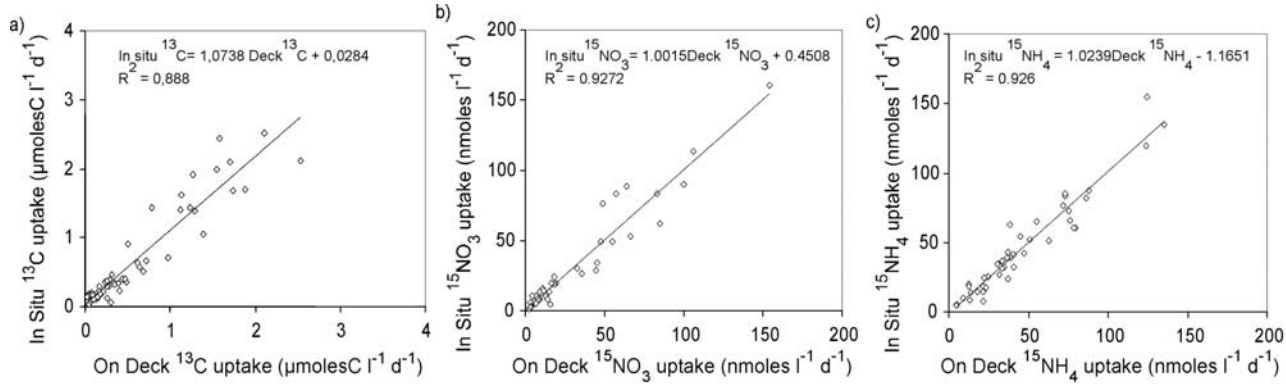

Figure 2. Results of the $^{15}N/^{13}C$ deck–in situ intercalibration experiment. (a) Primary production (µmoles C L^{-1} d^{-1}). (b) Nitrate assimilation (nmoles L^{-1} d^{-1}). (c) Ammonium assimilation (nmoles L^{-1} d^{-1}).

work, we corrected new production from measured nitrification rates, as illustrated in equation (6), where ρ_{NIT} from equation (4) represents nitrification and is assumed to balance the assimilation of regenerated nitrate formed during the incubation:

$$f = \frac{\rho(NO_3^-)}{[\rho(NO_3^-) + \rho(NH_4^+)]} \quad (5)$$

$$f = \frac{\rho(NO_3^-) - \rho_{NIT}}{[\rho(NO_3^-) + \rho(NH_4^+)]}. \quad (6)$$

[23] During the second leg of each cruise, an intercalibration experiment was carried out between "deck" and in situ incubations (Figure 2) for measurements of carbon, nitrate and ammonium assimilation (Figures 2a, 2b, and 2c). Results show a very close relationship between both methods, with differences generally lower than 10%.

3. Results

3.1. Hydrological Background

[24] Table 1 shows average properties of surface waters for stations located north and south of 41.5°N (Figure 1a), which is the approximate location of the hydrological front that characterizes the mode water subduction area [*Paillet and Arhan*, 1996]. During 2001, sea surface temperature (SST) varied from 13.8°C in winter to 21.6°C in late summer, with higher values in the southern area. This trend was also followed by sea surface salinity (SSS) data (Table 1).

[25] Vertical mixing (defined here as the depth level at which a change in potential density, σ, higher than 0.001 kg m^{-3} is observed in two consecutive determinations spaced by 5 m within a CTD cast) reached deeper layers in the northern area (143.6 ± 57 m (Table 1)) during POMME 1 (hereafter referred as P1), while in the southern area, winter mixing reached 124.1 ± 45 m. During POMME 2 (hereafter referred as P2), a general decrease in the depth of the mixed layer (MLD) was observed, but average values were slightly higher in the southern area (96.3 ± 40 m (Table 1)). The smallest difference between northern and southern areas was observed during POMME 3 (hereafter referred as P3), when MLD values varied between 27.8 ± 9 m in the south and 28.44 ± 10 m in the northern area (Table 1).

[26] The seasonal evolution of the euphotic layer (Z_{eu} [*Morel and Maritorena*, 2001]) is illustrated in Figure 3. During P1, Z_{eu} showed a homogeneous distribution, with average values close to 60 m in the entire zone. Maximum values were observed at 40°N (75 m) and also toward the northern extreme of the grid (~90 m). During P2, a general decrease in the thickness of the Z_{eu} was observed, and values varied between 45 m at 39°N to 50 m at 44.5°N. Being a light irradiance related parameter, this decrease in Z_{eu} implicates increased light energy during the spring season than during winter. During P3, the euphotic zone deepened (100–120 m) in stations located south of 41°N.

Table 1. Mean Values Per Cruise of Sea Surface Temperature (SST) and Sea Surface Salinity (SSS) for Northern and Southern Areas of the Programme Océan Multidisciplinaire Méso Echelle (POMME) Sampling Grid[a]

	POMME 1		POMME 2		POMME 3	
	South	North	South	North	South	North
SST, °C	13.9 ± 0.8	13.8 ± 0.7	14.6 ± 1.8	14.1 ± 0.8	21.6 ± 1.1	21.5 ± 1.1
SSS, psu	35.8 ± 0.1	35.8 ± 0.1	35.8 ± 0.07	35.8 ± 0.1	35.95 ± 0.2	35.97 ± 0.2
MLD, m	124.1 ± 45	143.6 ± 57	96.3 ± 40	90.5 ± 49	27.8 ± 9	28.4 ± 10
NO_3^-, µmoles L^{-1}	2.87 ± 0.2	5.84 ± 0.2	2.33 ± 0.5	5.01 ± 0.2	0.78 ± 0.1	1.94 ± 0.2
NO_2^-, µmoles L^{-1}	0.16 ± 0.01	0.12 ± 0.01	0.18 ± 0.06	0.22 ± 0.03	0.03 ± 0.03	0.05 ± 0.04
NH_4^+, µmoles L^{-1}	24.4 ± 2.4	10.7 ± 2	93.6 ± 29	96.08 ± 26.8	11.6 ± 4.3	7.85 ± 3.9

[a]MLD, mean values per cruise of the depth of the mixed layer (change in potential density (σ) higher than 0.001 kg m^{-3} in two consecutive determinations, spaced by 5 m, within a conductivity-temperature-depth cast). Nutrient data is expressed as a mean over the euphotic zone.

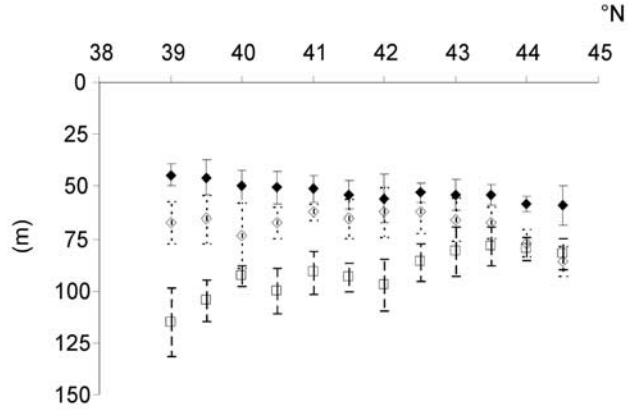

Figure 3. Latitudinal evolution of the average depth (m) of the euphotic layer (Z_{eu}): open diamonds, P1 (standard deviation in dotted line); solid diamonds, P2 (standard deviation in full line); open squares, P3 (standard deviation in dashed line) (H. Claustre et al., unpublished data, 2001).

Between 41°N and 42°N, Z_{eu} values were close to 100 m and decreased northward to reach minimal values (75 m) from 42.5°N to 44.5°N.

3.2. Seasonal and Spatial Variability in Biogeochemical Properties: Nutrients

[27] Nutrient concentrations, averaged over the Z_{eu} (Table 1), confirmed the north to south gradient described above for hydrological parameters. For all cruises, average NO_3^- concentrations were at least 40% higher in the northern part of the study area than in the south. Average surface values during P1 ranged from 5.84 ± 0.2 μmoles L^{-1} in the north to 2.87 ± 0.2 μmoles L^{-1} in the south, with extrema of 6.5 μmoles L^{-1} at 44.5°N and 2 μmoles L^{-1} at 39°N (Figure 4). During P2, average concentrations over the euphotic layer were 15% to 19% lower than during winter, which represents an average decrease of 2 μmoles L^{-1} in the surface layer between both cruises (Table 1). The smallest decrease in surface nitrate values was observed at the frontal zone (41°–42°N). In surface waters, data followed the same latitudinal evolution observed in winter, with average values reaching 2.33 ± 0.5 μmoles L^{-1} in the south and 5.01 ± 0.2 μmoles L^{-1} in the north (Table 1). The latitudinal distribution of surface nitrate concentrations showed minimal values close to 1 μmoles L^{-1} at 39°N (Figure 4), while northern surface values reached maximum average concentrations (5.5 μmoles L^{-1}) at 44.5 °N.

[28] During P3, average nitrate concentrations over the Z_{eu} were still higher in the northern area compared to the south. Maximum values reached 1.94 ± 0.2 μmoles L^{-1} (Table 1), while southern average values reached only 0.78 ± 0.1 μmoles L^{-1}. In surface waters, NO_3^- concentrations (Figure 4) were generally close to the detection limit.

[29] Surface NO_2^- concentrations were detectable during all cruises. During P1, nitrite values, averaged over the Z_{eu}, ranged between 0.12 ± 0.01 μmoles L^{-1} north of the frontal zone and 0.16 ± 0.01 μmoles L^{-1} in the south (Table 1). During P2, values in the northern area increased to 0.22 ± 0.03 μmoles L^{-1}, while southern average values showed little variation (0.18 ± 0.06 μmoles L^{-1}) compared to the winter season. During P3, nitrite concentrations were low compared to P1 and P2, and maximum values were observed in the northern area (0.05 ± 0.04 μmoles L^{-1}).

[30] Ammonium concentrations were generally higher in the southern area. During winter, values ranged between 10.7 ± 2 nmoles L^{-1} and 24.4 ± 2.4 nmoles L^{-1}. During spring, NH_4^+ concentrations showed a ninefold increase, with values ranging between 93.6 ± 29 nmoles L^{-1} in southern stations and 96.08 ± 26.8 nmoles L^{-1} in northern stations. The lowest NH_4^+ concentrations were observed during P3, when maximum values reached 11.61 ± 4.3 nmoles L^{-1} and minimum values were observed in the northern area (7.85 ± 3.9 nmoles L^{-1} (Table 1)).

[31] A detailed description of the evolution of temperature and salinity in the study area as well as the main characteristics of the mesoscale features sampled during the POMME experiment can be found in some companion papers [*Assenbaum and Reverdin*, 2005; *Fernández et al.*, 2005; *Mémery et al.*, 2005; *Reverdin et al.*, 2005].

[32] As outlined by *Fernández* [2003] and *Fernández et al.* [2005], nutrient consumption between winter and spring resulted in a nutrient depleted zone that was initially observed in the southwestern part of the grid and in the vicinity of the frontal zone. Rapidly, nutrients were depleted in the northern area as well, along transects 18°–19.3°W [*Fernández et al.*, 2005]. The presence of a SWODY-type eddy [*Pingree and Le Cann*, 1992] from P1 through P3 in the northern area (hereafter referred as A1 [*Le Cann et al.*, 2005; J.-C. Gascard et al., unpublished data, 2001]) and an anticyclone resulting from meddy influence (hereafter referred as A2 [*Le Cann et al.*, 2005]) in the southern area (Figures 7a and 7b) resulted in higher NO_3^- concentrations in waters inside and in the vicinity of both structures from January to early April [*Fernández et al.*, 2005]. During P3, eddy A1 (Figure 7c) was carrying northeast Atlantic Mode Water and showed a cold core "mode water eddy" structure [*Pingree and Le Cann*, 1992; *McGillicuddy et al.*, 1999] which influenced the seasonal and permanent thermocline creating a lens of water containing 7–9 μmoles L^{-1} of NO_3^- in its core [*Fernández et al.*, 2005]. A weaker but continuous impact in nutrient distribution was observed inside a

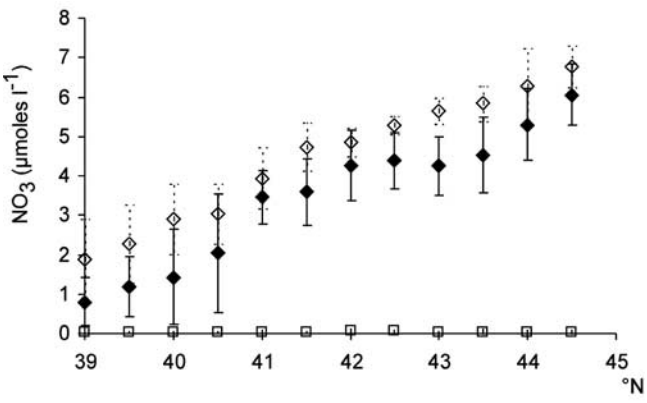

Figure 4. Average values of surface NO_3^- (μmoles L^{-1}) in the main study area (39°N–44.5°N), plotted against latitude. Open diamonds, P1 (standard deviation in dotted line); solid diamonds, P2 (standard deviation in full line); open squares, P3 (standard deviation in full line).

Table 2. Mean Values Per Cruise of Carbon and Nitrogen Rates, Integrated Over 80 m ($\Sigma\rho^{13}C$, $\Sigma\rho^{15}NO_3$, $\Sigma\rho^{15}NH_4$) and Maximum Surface Values Per Cruise of Carbon and Nitrogen Uptake Rates ($\rho^{13}C$, $\rho^{15}NO_3$, $\rho^{15}NH_4$)

	Unit	POMME 1	POMME 2	POMME 3
$\Sigma\rho^{13}C$	mmoles m^{-2} d^{-1}	38	103	35
$\rho^{13}C$	μmoles L^{-1} d^{-1}	1.64	7.81	1.27
$\Sigma\rho^{15}NO_3$	mmoles m^{-2} d^{-1}	1.77	3.48	0.94
$\rho^{15}NO_3$	nmoles L^{-1} d^{-1}	142	277.1	52.4
$\Sigma\rho^{15}NH_4$	mmoles m^{-2} d^{-1}	1.89	4.68	2.95
$\rho^{15}NH_4$	nmoles L^{-1} d^{-1}	69	174.4	80

cyclonic eddy (hereafter referred as C4 [*Le Cann et al.*, 2005]), north of the frontal zone (Figures 7a, 7b, and 7c).

3.3. Primary Production ($\rho^{13}C$)

[33] Average profiles of primary production for the entire POMME area were vertically integrated over 80 m (i.e., the deepest level of the production experiments) using the trapezoidal method. Winter integrated primary production (38 mmoles m^{-2} d^{-1} (Table 2)) was very close to the rate obtained during the late summer season (35 mmoles m^{-2} d^{-1} (Table 2)). Spring integrated primary production reached 103 mmoles m^{-2} d^{-1} (Table 2).

[34] During the first half of the year, seasonal variability in primary production was concentrated in the first 40 m of the water column, as it can be observed in the average profiles of primary production plotted in Figure 5a. In winter, average surface values were close to 0.88 ± 0.4 μmoles L^{-1} d^{-1} (Figure 5a), although surface rates could reach 1.64 μmoles L^{-1} d^{-1} (e.g., station 54, 40°N, 18.67°W (Table 2)). Maximum rates (up to 2.25 μmoles L^{-1} d^{-1}) were observed at 20 m depth at station 53 (40.5°N, 18.67°W). In spring, surface average values showed almost a fourfold increase (3.52 ± 1.4 μmoles L^{-1} d^{-1} (Figure 5a)), and reached maximum rates (up to 7.81μmoles L^{-1} d^{-1} (Table 2)) at station 68 (40.5°N, 20°W). During the late summer season, rates of primary production showed an homogeneous profile, with surface values close to winter carbon uptake rates (0.77 ± 0.2 μmoles L^{-1} d^{-1} (Figure 5a)), and average values close to 0.56 μmoles L^{-1} d^{-1} between the surface and 40 m depth. In surface waters, the maximum rate (1.27 μmoles L^{-1} d^{-1} (Table 2)) was measured at station 66 (44.5°N, 19.3°W), while at station 21 (43°N, 17.3°W) a subsurface maximum of 1.73 μmoles L^{-1} d^{-1} was measured at 40 m depth. Below 50 m depth, primary production rates were lower than 0.4 μmoles L^{-1} d^{-1} for all cruises (Figure 5a).

[35] During P1, southern and northern stations showed little difference in carbon uptake rates (Figure 6a). However, spatial variability in primary production was intense during P2 (Figure 6a). Indeed, southern stations showed average surface values 35% higher (4.25 μmoles L^{-1} d^{-1}) compared to the north (2.78 μmoles L^{-1} d^{-1}). In deeper waters (e.g., 40 m depth (Figure 6a)), northern stations attained primary production rates (∼1.2 μmoles L^{-1} d^{-1}) that exceeded southern stations by 50%. During P3 (Figure 6b), rates of primary production reached 1.01 μmoles L^{-1} d^{-1} in the northern area (Figure 6b), while in the south, rates oscillated between 0.5 and 0.73 μmoles L^{-1} d^{-1} in the top 40 m (Figure 6b).

[36] In Figure 7, every primary production profile was integrated over 80 m depth, and confronted to the mesoscale geostrophic current field. During all cruises, values of integrated primary production were higher in the front – eddy interaction zones, and in the vicinity of the major mesoscale features described in section 3.2. During P1 (Figure 7a), higher values (up to 74.5 mmoles C m^{-2} d^{-1}) were observed along transects located along 18°W and 18.67°W. During P2, values were considerably higher and maximum rates (∼238 mmoles C m^{-2} d^{-1}) were concentrated in the southwestern region (station 68 at 40.5°N, 20°W (Figure 7b)), and in the vicinity of the anticyclone A2 (40°N, 20°W). In the northern region, values between 100 and 150 mmoles C m^{-2} d^{-1} were associated with eddies C4 and A1 and the turbulent zone between them (Figure 7b). In late summer (Figure 7c), primary production rates were generally lower than 60 mmoles C m^{-2} d^{-1}, and the highest values (68.9 mmoles C m^{-2} d^{-1}) were observed at station 21 (43°N, 17.3°W), which was located in the vicinity of the anticyclonic eddy A1 (Figure 7c).

3.4. Nitrogen Uptake

3.4.1. New Production (ρNO_3)

[37] During winter, average surface ρNO_3 reached 31 nmoles L^{-1} d^{-1} and increased to 54 nmoles L^{-1} d^{-1} at 20 m depth (Figure 5b). Maximum rates were observed at station 63 (42°N, 19.3°W (Table 2)), where surface values reached 142 nmoles L^{-1} d^{-1} and increased to 225.3 nmoles L^{-1} d^{-1} at 20 m depth. In deeper layers, average rates of nitrate assimilation in the entire study area decreased with depth and reached 2 nmoles L^{-1} d^{-1} at 80 m depth (Figure 5b).

[38] In Figure 8, ρNO_3 profiles were vertically integrated over 80 m and associated to the geostrophic current field. Values of integrated ρNO_3 were generally below 3 mmoles m^{-2} d^{-1} (Figure 8a). However, stronger values were observed in the northern area, particularly in the vicinity of eddy C4 (>7 mmoles m^{-2} d^{-1} (Figure 8a)). In the southern area (and near anticyclone A2), values reached 4 to 5 mmoles m^{-2} d^{-1}.

[39] During P2, average surface ρNO_3 reached 130 nmoles L^{-1} d^{-1} (Figure 5b), while rates below 50 m depth were generally close to zero (Figure 5b). Maximum surface values (277.1 nmoles L^{-1} d^{-1} (Table 2)) were observed at station 53, located at 41.5°N; 19.3°W. Concerning integrated values, the highest integrated ρNO_3 rates (∼8–9 mmoles m^{-2} d^{-1}) were observed in the southwestern part of the study area (Figure 8b). Northern rates were generally lower than 5 mmoles m^{-2} d^{-1}, except for the area near eddies C4 and A1, where values could reach 7 mmoles m^{-2} d^{-1} (Figure 8b).

[40] During P3, vertical profiles showed average ρNO_3 values close to 16 nmoles L^{-1} d^{-1} between the surface and 80 m depth (Figure 5b). However, maximum values reached 52.4 nmoles L^{-1} d^{-1} (Table 2) at station 21, located inside

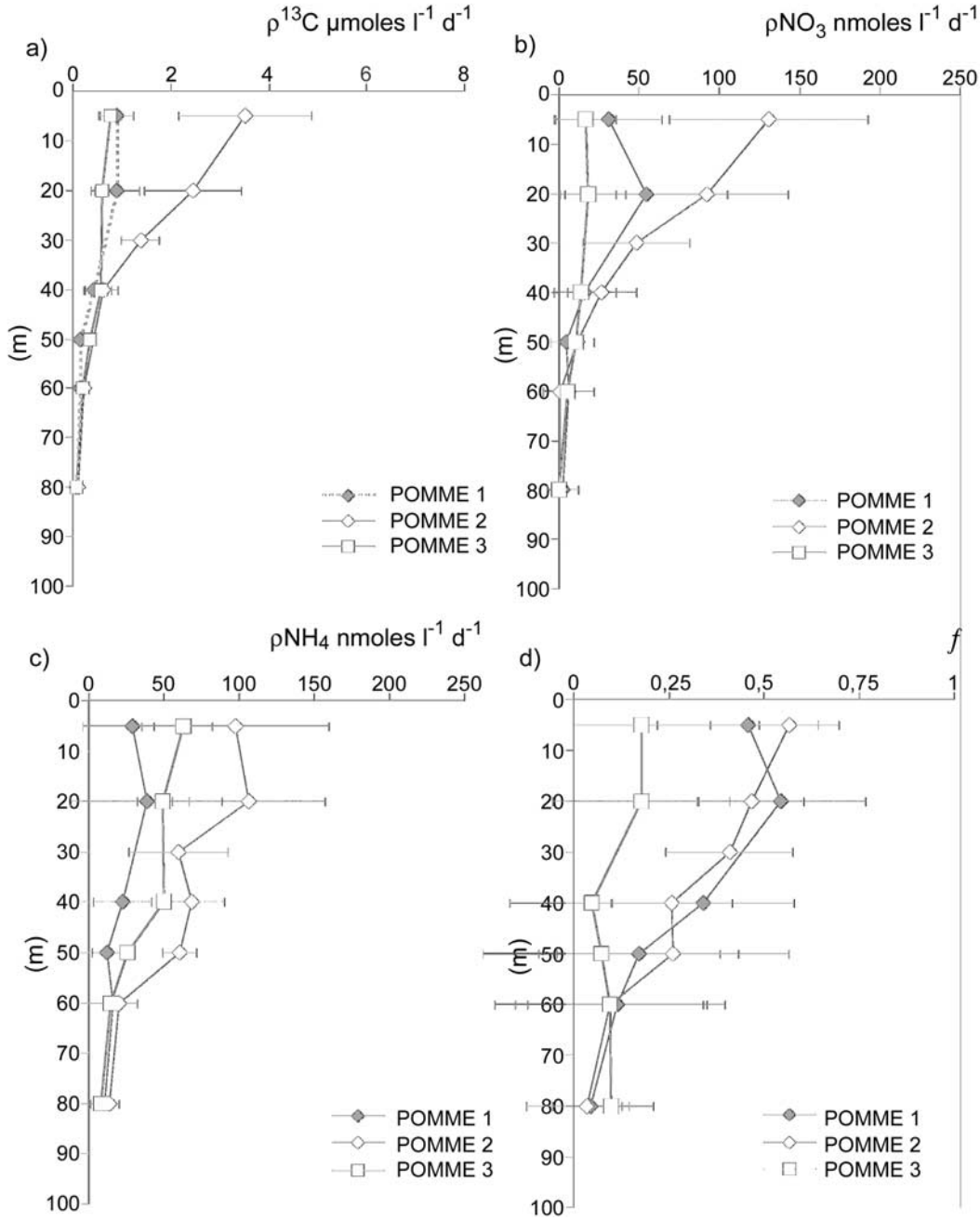

Figure 5. Vertical profiles per cruise of average (a) primary production, (b) nitrate assimilation, (c) ammonium assimilation, and (d) *f* ratio. Open diamonds, P1; solid diamonds, P2; open squares, P3. Standard deviation is represented by the full line.

the domain of eddy A1. Integrated ρNO_3 showed a west to east gradient and, as seen for primary production, higher values were observed in the northeastern part of the grid (up to 3 mmoles m^{-2} d^{-1}), especially near the domain of eddy A1 (Figure 8c).

3.4.2. Regenerated Production (ρNH_4)

[41] During winter, vertical profiles of average ammonium assimilation (Figure 5c) showed values close to 29 nmoles L^{-1} d^{-1} in surface waters, and increased to 38 nmoles L^{-1} d^{-1} at 20 m depth (Figure 5c). A secondary peak was observed at 60 m depth, with average ρNH_4 values of 16 nmoles L^{-1} d^{-1} (Figure 5c). The highest ammonium uptake rates were observed at 20 m depth at station 54 (71.2 nmoles L^{-1} d^{-1}), which was located near the frontal zone (40°N, 18.7°W) and at station 2 (80 nmoles L^{-1} d^{-1}) located in the southeastern part of the grid (39.5°N, 16.7°W). Integrated values of ρNH_4 were associated to the geostrophic current field in Figure 8. Values obtained were generally lower than 3 mmoles m^{-2} d^{-1}, except for two maxima of approximately 4 mmoles m^{-2} d^{-1} observed on both sides of the frontal zone, along the 18.67°W transect (Figure 8d).

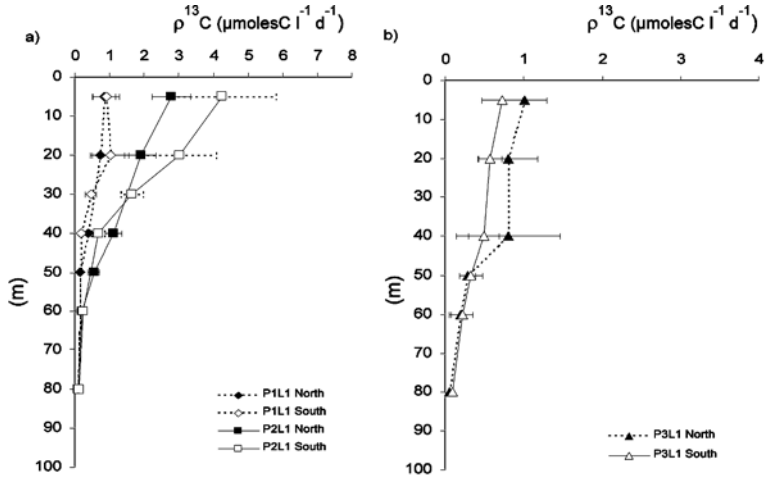

Figure 6. Vertical profiles per cruise of primary production in southern and northern areas of the POMME zone.

[42] During spring, average rates of ammonium uptake in surface waters were higher than winter values and reached 97.36 nmoles L^{-1} d^{-1} (Figure 5c), with a maximum value of 174.4 nmoles L^{-1} d^{-1} in the northwestern part of the grid (44°N, 16.6°W). At 20 m depth, average values were close to 106 nmoles L^{-1} d^{-1} (Figure 5c) while maximum values exceeded surface uptake rates at the frontal zone and reached 195 nmoles L^{-1} d^{-1} and 307 nmoles L^{-1} d^{-1} at stations 58 (41.5°N, 18.6°W) and 59 (41.5, 19.3°W) respectively. Another subsurface peak was observed near 40 m depth, with average values close to 68 nmoles L^{-1} d^{-1} and maximum values of 184 nmoles L^{-1} d^{-1} at station 68, located near the location of anticyclone A2 (40.5°N, 20°W). Integrated values of ρNH_4 (Figure 8e) were higher in the southern area (to ~8 mmoles m^{-2} d^{-1}). High integrated rates (up to 7 mmoles m^{-2} d^{-1}) were also observed in the north, particularly in stations located in the area between eddies C4 and A1.

[43] During P3, average ρNH_4 (Figure 5c) showed surface rates of 63 nmoles L^{-1} d^{-1} in surface waters, which is almost twice the average values for the winter season. East of 18°W, maximum values could exceed 80 nmoles L^{-1} d^{-1} in the first 20 m depth (Table 2). In deeper layers, average rates decreased with depth to 50 nmoles L^{-1} d^{-1} at 40 m depth, and finally reached 15 nmoles L^{-1} d^{-1} below 40 m (Figure 5c).

[44] Integrated ρNH_4 uptake rates (Figure 8f) were higher at stations located east of 17.5°W. Maximum rates reached 4.1 mmoles m^{-2} d^{-1} in the east (40°–43°N, 18°–16°W (Figure 8f)) while western values were lower than 2.5 mmoles m^{-2} d^{-1}. Stations located in the vicinity of eddy A1 showed rates higher than 3 mmoles m^{-2} d^{-1} (Figure 8f).

3.5. *f* Ratio

[45] The vertical distribution of the *f* ratio during P1 (Figure 5d) showed average values close to 0.45 in the surface layer, and lower values (0.26) at 50 m depth. This trend indicates that new production was supporting biological activity in the surface, while in deeper layers the regenerated forms of nitrogen can support a significant fraction of the nitrogen uptake. Nitrification rates observed during this cruise showed a significant increase below 30 m depth (our own data, not shown). During P2 (Figure 5d), average *f* values increased to 0.56 in surface waters although minimum values of 0.2 were observed. In deeper layers, average values were close to 0.17 between 40 and 50 m depth. This trend coincides with high rates of regenerated production observed at this level. During P3, *f* was close to 0.25 between the surface and 30 m depth (Figure 5d). Beyond this level, average values did not exceed 0.1.

4. Annual Carbon Budget for the Programme Océan Multidisciplinaire Méso Echelle Area

[46] In order to provide an estimation of the annual carbon budget for the POMME study area, calculations must deal with the lack of data between cruises, when only moored or drifting instruments provided hydrographical and physical parameters in the study area.

4.1. Estimating the Length of Each Season

[47] The annual productive cycle will be considered as composed by three distinct periods: winter, spring and intermediate seasons.

[48] The winter season is considered as a 49 day period (Table 3), representing the duration of the winter cruise P1 (including legs 1 and 2; i.e., 31 January–19 March 2001).

[49] The spring season includes the time between the end of the winter season and the moment when all nutrients were depleted in the surface layer. However, at the end of the second leg of the spring cruise (8 May 2001), nitrates were not entirely depleted in the northern area and therefore the actual date of total depletion of nutrients is unknown. To estimate this date, we assumed that nitrate consumption over the study area was at a constant rate. This overall regional rate is obtained from the average nitrate concentrations during the first (4.78 μmoles L^{-1}) and second (1.78 μmoles L^{-1}) legs of the spring cruise (P2).

[50] With such a constant rate, the estimated total depletion of NO_3^- should have taken place about 12 days after the end of the second leg of the cruise P2. Therefore the length of the spring season is 59 days (Table 3).

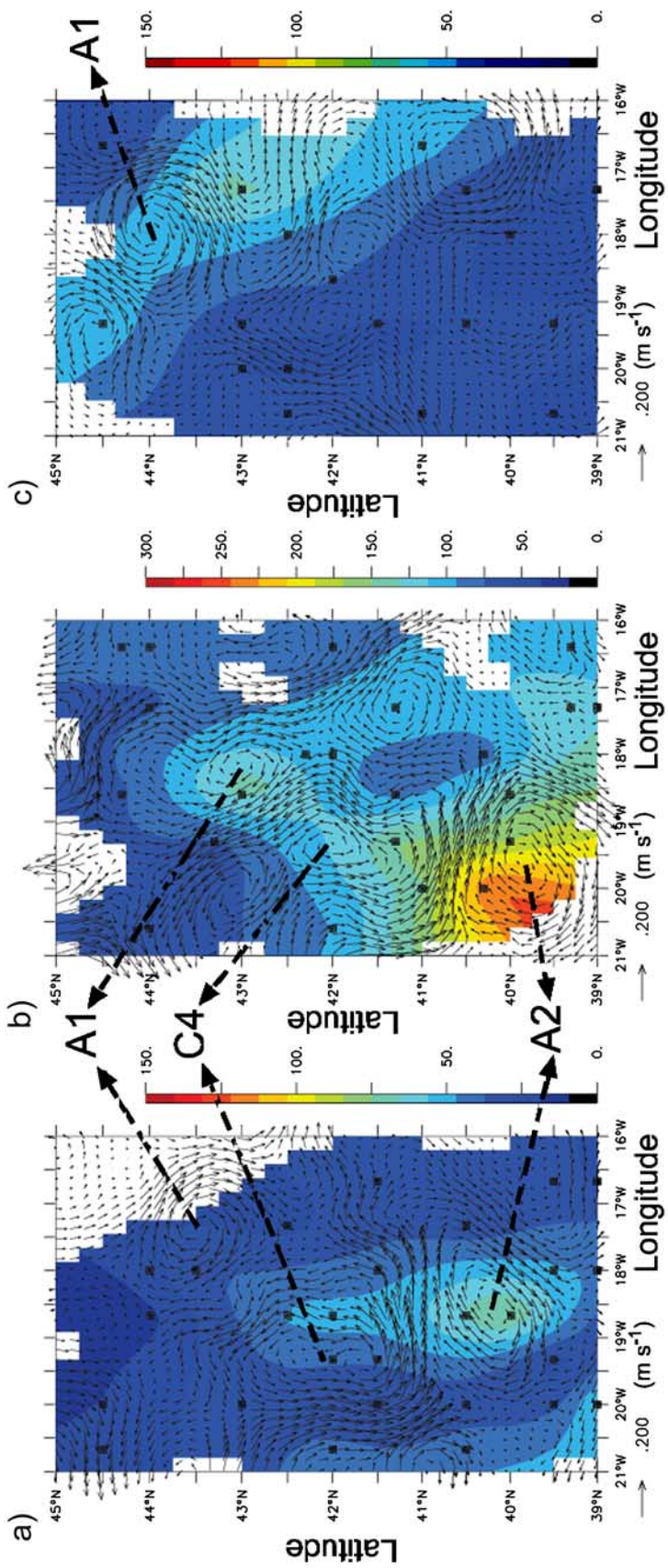

Figure 7. Maps showing integrated primary production (mmoles C m^{-2} d^{-1}) during (a) P1, (b) P2, and (c) P3.

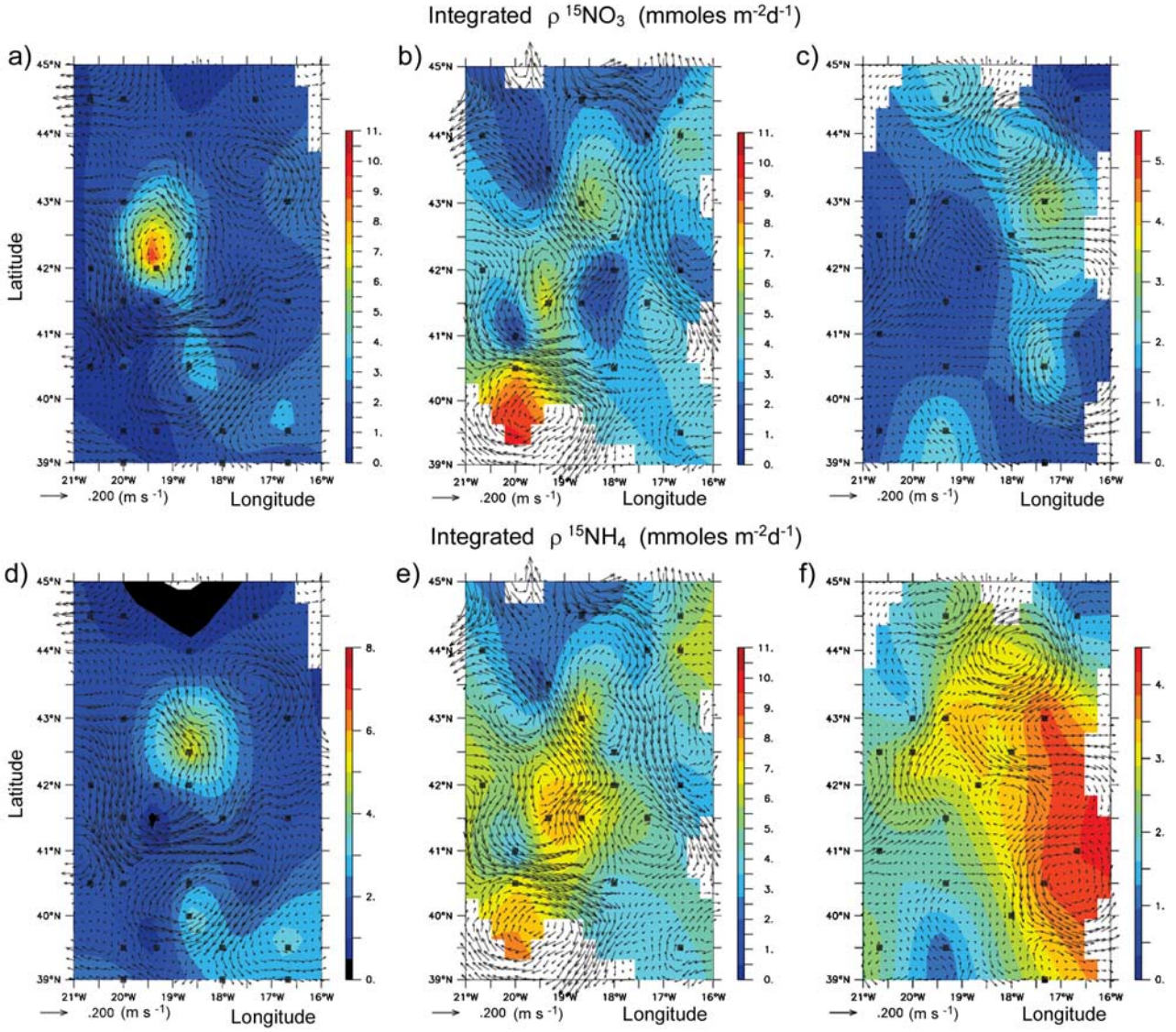

Figure 8. Maps showing nitrate uptake rates integrated over 80 m (mmoles m^{-2} d^{-1}) during (a) P1, (b) P2, and (c) P3. Ammonium uptake rates integrated over 80 m during (d) P1, (e) P2, and (f) P3.

[51] The rest of the year (i.e., 257 days) will be considered as the intermediate season, which includes the late summer period sampled during P3 and ends at the date preceding the last phase of winter conditioning.

4.2. Annual Carbon Fixation Rates: Spatial Variability

[52] Given the north to south gradient observed in biogeochemical parameters, it is important to determine if the initial nutrient stock measured in winter could support the observed uptake rate on both sides of the front, or if an alternative source of nitrogen was supporting primary production.

[53] Northern and southern average rates of carbon new production ($\rho^{13}C * f$) were divided by the corresponding C:N ratio (defined here as total carbon to total nitrogen, with ammonium assimilation values corrected for isotopic dilution) for every depth level and every cruise. This allowed obtaining the assimilated nitrate for each season in both areas of the POMME zone. The results were assimilated to the length of each season and integrated over 80 m depth. The annual amount of nitrate assimilated in the north reached 494 mmoles m^{-2} yr^{-1} (Table 3). The initial stock of NO_3^- measured during P1 reached 463 mmoles m^{-2} (Table 3), and approximately balance the annual nitrate assimilation observed north of the frontal zone.

[54] The southern area showed an annual amount of 401 mmoles m^{-2} yr^{-1} of assimilated nitrate (Table 3). The initial stock of NO_3^- measured in the southern area only reached 260 mmoles m^{-2} (Table 3). This 35% deficit in the observed rates of annual nitrate uptake may result from consumption of nutrient before our determination of the beginning of the spring season, helped by an earlier stabilization of the water column compared to northern conditions. In addition, the active regenerated production and higher NH_4^+ concentrations measured in the south at all times of the year suggest an alternative source of nitrogen available in the photic zone, the origin of which may be related to export production earlier in the year. Indeed, it is

Table 3. Annual Carbon Budgets for the POMME Study Area[a]

	Unit	Winter Season 49 Days	Bloom Season 59 Days	Intermediate Season 257 Days	Annual Results
Daily $\Sigma\rho^{13}C$	mmoles m^{-2} d^{-1}	38	103	35	
Daily $\Sigma(\rho^{13}C*f)$	mmoles m^{-2} d^{-1}	16	48	8	
Daily Σ $(\rho^{13}C*f)$ north	mmoles m^{-2} d^{-1}	17	41	10	
Daily Σ $(\rho^{13}C*f)$ south	mmoles m^{-2} d^{-1}	14	64	7	
Seasonal $\Sigma(\rho^{13}C*f)$	mmoles m^{-2} t^{-1}	784	2832	2056	
Seasonal Σ $(\rho^{13}C*f)$ north	mmoles m^{-2} t^{-1}	833	2419	2570	
Seasonal Σ $(\rho^{13}C*f)$ south	mmoles m^{-2} t^{-1}	686	3776	1799	
Annual $\Sigma(\rho^{13}C*f)$	moles C m^{-2} yr^{-1}				5.7
Seasonal ρNO_3	mmoles m^{-2} t^{-1}	65	250	196	511
Seasonal ρNO_3 north	mmoles m^{-2} t^{-1}	87	184	223	494
Seasonal ρNO_3 south	mmoles m^{-2} t^{-1}	50	277	74	401
Winter ΣNO_3 pool	mmoles m^{-2}				352
Northern winter ΣNO_3 pool	mmoles m^{-2}				463
Southern winter ΣNO_3 pool	mmoles m^{-2}				260
Annual carbon assimilation $T\Sigma\rho^{13}C$	moles m^{-2} yr^{-1}				16.9

[a] $\Sigma^{13}C$, primary production rates integrated over 80 m; $\Sigma^{13}C*f$, carbon production resulting from nitrate assimilation for the POMME area. It is obtained by multiplying average profiles of ^{13}C and the f ratio and integrating the resulting values. ρNO_3, the seasonal nitrate assimilation obtained from average profiles of primary production, f ratio, and C: N ratio and integrated over 80 m depth; winter ΣNO_3^- pool, represents the nitrate pool measured during POMME 1, integrated over 80 m depth.

possible that recently exported nitrogen, remineralized into nitrate may account for a not yet determined portion of the deficit observed.

[55] These results confirm the definition of two distinct regimes inside the study area that were separated at 41°–42°N by the location of the hydrological front [*Fernández et al.*, 2005]. In fact, in the case of the northern area, the first cruise (P1) took place approximately at the end of the prebloom conditioning. On the contrary, nutrient consumption in the southern region is likely to have begun before the winter cruise P1 or to be fuelled as well by regenerated forms of nitrogen than by new production.

4.3. Annual Primary Production Budget

[56] The annual carbon assimilation budget for the entire POMME area can be estimated using equation (7):

$$\sum {}^{13}C_{(\text{moles C m}^{-2}\,\text{y}^{-1})} = \left(\left(\sum {}^{13}Ct_1 \times \Delta t_1\right) + \left(\sum {}^{13}Ct_2 \times \Delta t_2\right) + \left(\sum {}^{13}Ct_3 \times \Delta t_3\right)\right),$$

where $\Sigma^{13}C_{tx}$ is the integrated primary production in daily rates (moles C m^{-2} d^{-1}) for t_1: winter, t_2: spring and t_3: intermediate season. Δt_x represents the time length of each season, in days.

[57] We obtain 16.9 moles C m^{-2} yr^{-1} (Table 3). There is scarce information on annual estimations of primary production that can be used to place the results of this study in a wider perspective. Most of the estimates come from indirect measurements, such as satellite derived chlorophyll, and light-photosynthesis models [*Morel and André*, 1991; *Antoine et al.*, 1995]. *Nixon* [1995] assigned to oligotrophic, mesotrophic and eutrophic areas, annual carbon uptake rates of <8.3, 8.3 to 25 and 25 to 41.6 moles C m^{-2} yr^{-1}, respectively. Following this criteria, the POMME area could be considered as a mesotrophic region, with production rates considerably higher than the estimates made by *Longhurst et al.* [1995] for the eastern part of the North Atlantic Subtropical Gyre (NASE, ~10 moles C m^{-2} yr^{-1}).

[58] Using our primary production measurements and estimates of f ratio, we calculated the carbon new production for the daily average profile of each cruise. The resulting new carbon production profile was integrated over 80 m and the resulting amount was then assimilated to the theoretical length of each season. By using this method, we find that new carbon production in the study area was 5.7 moles C m^{-2} yr^{-1} (Table 3).

5. Discussion

5.1. General Overview

[59] During 2001, nutrient depletion in the study area probably started in February and was associated with early biological production south of 41°–42°N. At that moment, the northern area was experiencing the last stage of winter conditioning. The time lag between these two regimes was on the order of 20 to 30 days in the beginning of the 2001 bloom.

[60] During the POMME survey, rates of new nitrate assimilation were lower than expected [*Fernández*, 2003] due to intense nitrification activity that accounted for regenerated production which in turn fueled the surface layer with recycled nitrate available for phytoplankton uptake. Consequently, seasonal average values of the f ratio for the entire study area ranged between 0.2 and 0.56 (Figure 5d), although extrema could reach 0.75 and 0.1. These results suggest that, although nitrate is important as a source of nitrogen in the POMME area, the regeneration compartment was also active during the year and was closely associated to primary production. The study of microbial communities confirms what was observed for $\rho^{13}C$ and $\rho^{15}NO_3$. Indeed, biomass of heterotrophic bacteria was high and its variability was often related to front-eddy and eddy-eddy interaction zones, at least during spring [*Thyssen et al.*, 2005] and late summer (C. Fernández, manuscript in preparation, 2005). Moreover, even if the composition of the microbial community was dominated by autotrophs from winter through late summer, the contribution of large micro phytoplankton cells to biological production was small [*Maixandeau et al.*, 2005].

[61] Primary production rates obtained during our study (35–103 mmoles m^{-2} d^{-1}) are in the same range of values obtained during the NABE experiment by *Lochte et al.* [1993] and *Bury et al.* [2001]. Results presented by *Bender et al.* [1992] and *Chipman et al.* [1993] match nicely our estimations for the spring season (103 mmoles m^{-2} d^{-1} and 106 mmoles m^{-2} d^{-1}, respectively). However, our spring primary production rates are slightly higher than the estimations obtained by *Martin et al.* [1993] during NABE (90 mmoles m^{-2} d^{-1}). Our results are also considerably higher than the rates estimated by *Donald et al.* [2001] during the PRIME experiment at 44.46°N (28 mmoles m^{-2} d^{-1}) and 40.63 (7.6 mmoles m^{-2} d^{-1}). This significant difference may be explained by the seasonal and annual variability between the spring cruise of the POMME study (April–May 2001) and the PRIME study, which was carried out in July 1996. Indeed, it is widely accepted that during the summer season, primary production is likely to drop, which may affect annual estimations of carbon and nitrogen uptake. Unfortunately, no data is available for our study during this particular season.

[62] Concerning the *f* ratio, the corrections we performed on new and regenerated production support the importance of making a clear distinction between new and regenerated sources of nitrogen when calculating the fraction of primary production that is effectively available for export. Average uncorrected *f* ratio ranged between 0.3 and 0.7 along the year (our own unpublished data). This values are 20–30% higher than values of *f* obtained by correcting new production from nitrification (0.2–0.56, this study). Our corrected *f* ratio is also considerably lower than those presented by *Bury et al.* [2001] in 1993 (0.45–0.8), for which the classical calculation of *Dugdale and Goering* [1967] was applied. For the same latitude range of the POMME area, *Donald et al.* [2001] reported ammonium uptake rates (1.2–4.8 mmol N m^{-2} d^{-1}) corrected from regeneration processes that are in the same range as our estimates for the winter and late summer seasons (3–4 mmoles m^{-2} d^{-1}). The *f* ratios obtained by *Donald et al.* [2001] also coincide with those presented in this work. During NABE, *Martin et al.* [1993] took nitrogen regeneration processes into account and estimated *f* ratio values on the order of 0.46, which are close to our estimates for the spring season.

[63] This study raises an important issue in estimating global new production, which is the use of values of the *f* ratio that have an inherent inaccuracy [*Koblentz-Mishke et al.*, 1970; *Eppley and Peterson*, 1979; *Wirtky*, 1981; *Platt and Harrison*, 1985; *Dugdale et al.*, 1992]. Indeed, *Chavez and Barber* [1987] stated that new production estimates based on primary production and an overestimated *f* ratio can explain the new production deficit in the model of *Eppley and Peterson* [1979]. This study responds to the need of accurate estimations of the *f* ratio, previously stressed by other authors [*Chavez and Barber*, 1987; *Murray et al.*, 1989; *Dugdale et al.*, 1992]. It also provides an annual new production budget that is more realistic than former estimates for which regeneration processes were not quantified.

5.2. Role of Mesoscale Activity

[64] The possible role of mesoscale structures for stimulating biological production cannot be fully evidenced in this study. There are, however, some interesting characteristics of the observed anticyclonic structures that deserve to be pointed out.

[65] During year 2001, primary production was particularly high in frontal – eddy interaction zones, as well as in the domain of anticyclones A1 and A2. This is justified by the enhanced availability of both nutrients and light due to physical forcing (e.g., "eddy pumping" and mode water transport).

[66] In winter, high primary production values were found between the 18°W and 19°W transects, and were also associated with the location of anticyclone A2. The depth of the mixed layer in that zone was lower than in the northern part of the study area and this eddy was located in what would later become the most productive part of the study area. In fact, the anticyclone A2 showed higher nutrient concentrations in its core since the beginning of winter and through the end of spring [*Fernández et al.*, 2005]. In the northern area, anticyclonic eddy A1 showed a marked evolution during the year and its effect on nutrient distribution was important since the beginning of the spring and became even stronger in late summer, when light penetration was more important and mixing was almost absent in its core. Concerning the origin of the assimilated nitrate inside A1 and A2, during the second legs of P1 and P2, measures of nitrification revealed that a significant fraction of the available nitrate in the surface layer of both eddies (A1 and A2) had its origin in nitrification (unpublished data), suggesting that mesoscale anticyclonic systems during POMME could be sustained for both new and regenerated production [*Fernández*, 2003].

6. Conclusion

[67] Rather than an isolated and intense event, the bloom in the northeast Atlantic basin was a gradual process in 2001, whose evolution followed mesoscale patterns with a temporal scale of the order of several weeks.

[68] This study confirms previous observations proposing a northward migration of the bloom [*Siegel et al.*, 1990; *Frazel and Berberian*, 1990; *Harrison et al.*, 1993], that starts between February and March in southern latitudes and in late summer (July/August) at high latitudes. The migration of the bloom is likely to be based on the progression of optimal conditions of light and temperature at a large scale, modulated by mesoscale processes.

[69] Despite of an efficient regeneration system that was active all through the year, the POMME area showed a positive annual flux of carbon from the atmosphere to the ocean. This zone, although small within the context of the North Atlantic Basin, can therefore be confirmed as a local carbon sink of carbon for the atmosphere as stated in former studies in the northeast Atlantic [*Takahashi et al.*, 1995].

[70] **Acknowledgments.** The POMME program was managed by L. Mémery and G. Reverdin. Data concerning euphotic layer depth was kindly provided by H. Claustre and J. Ras. Special thanks go to B. Boudjellal for his valuable help during P2 and to J. Cunningham for his valuable comments. We thank the referees and the Associate Editor, who helped enormously to improve the manuscript.

References

Allen, C. B., J. Kanda, and E. A. Laws (1996), New production and photosynthetic rates within and outside a cyclonic mesoscale eddy in North Pacific subtropical gyre, *Deep Sea Res., Part II*, *43*, 917–936.

Álvarez, M., A. F. Ríos, F. F. Pérez, H. L. Bryden, and G. Rosón (2003), Transports and budgets of total inorganic carbon in the subpolar and temperate North Atlantic, *Global Biogeochem. Cycles*, *17*(1), 1002, doi:10.1029/2002GB001881.

Antoine, D., A. Morel, and J.-M. André (1995), Algal pigment distribution and primary production in the eastern Mediterranean as derived from coastal zone color scanner observations, *J. Geophys. Res.*, *100*, 16,193–16,209.

Armstrong, F. A. J., C. R. Stearns, and J. D. H. Strickland (1967), The measurement of upwelling and subsequent biological processes by means of the Technicon AutoAnalyzer and associated equipment, *Deep Sea Res.*, *14*, 381–389.

Assenbaum, M., and G. Reverdin (2005), Near real-time analyses of the mesoscale circulation during the POMME experiment, *Deep Sea Res.*, in press.

Aufdenkampe, A. K., J. J. McCarthy, M. Rodier, C. Navarrette, J. Dunne, and J. W. Murray (2001), Estimation of new production in the tropical Pacific, *Global Biogeochem. Cycles*, *15*, 101–113.

Aufdenkampe, A. K., J. J. McCarthy, C. Navarrette, M. Rodier, J. Dunne, and J. W. Murray (2002), Biogeochemical controls on new production in the tropical pacific, *Deep Sea Res., Part II*, *49*, 2619–2648.

Bender, M., H. Ducklow, J. Kiddon, J. Marra, and J. Martin (1992), The carbon balance during the 989 spring bloom in the North Atlantic Ocean, 47°N, 20°W, *Deep Sea Res., Part A*, *39*, 1707–1725.

Bury, S. J., P. W. Boyd, T. Preston, G. Savidge, and N. J. P. Owens (2001), Size-fractionated primary production and nitrogen uptake during a North Atlantic phytoplankton bloom: Implications for carbon export estimates, *Deep Sea Res., Part I*, *48*, 689–720.

Chavez, F., and R. Barber (1987), An estimate of new production in the equatorial Pacific, *Deep Sea Res., Part A*, *34*, 1229–1243.

Chipman, D. W., J. Marra, and T. Takahashi (1993), Primary production at 47°N 20°W in the North Atlantic Ocean: A comparison between ^{14}C incubation method and the mixed layer C budget, *Deep Sea Res., Part II*, *40*, 151–169.

Diaz, F., and P. Raimbault (2000), Nitrogen regeneration and dissolved organic nitrogen release during spring in a NW Mediterranean coastal zone (Gulf of Lions): Implications for the estimation of new production, *Mar. Ecol. Prog. Ser.*, *197*, 51–65.

Donald, K. M., I. Joint, A. P. Rees, E. Malcom, S. Woodward, and G. Savidge (2001), Uptake of carbon, nitrogen and phosphorus by phytoplankton along the 20°W meridian in the NE Atlantic between 57.5°N and 37°N, *Deep Sea Res., Part II*, *48*, 873–897.

Dore, J. E., and D. M. Karl (1996), Nitrification in the euphotic zone as a source of nitrite, nitrate, and nitrous oxide at Station ALOHA, *Limnol. Oceanogr.*, *41*, 1619–1628.

Ducklow, H. W., and R. P. Harris (1993), Introduction to the JGOFS North Atlantic Bloom Experiment, *Deep Sea Res., Part II*, *40*, 1–8.

Dugdale, R. C., and J. J. Goering (1967), Uptake of new and regenerated forms of nitrogen in primary productivity, *Limnol. Oceanogr.*, *12*, 196–206.

Dugdale, R. C., and F. P. Wilkerson (1986), The use of ^{15}N to measure nitrogen uptake in eutrophic oceans, experimental considerations, *Limnol. Oceanogr.*, *31*, 673–689.

Dugdale, R. C., F. P. Wilkerson, R. T. Barber, and F. P. Chavez (1992), Estimating new production in the equatorial Pacific Ocean at 150°W, *J. Geophys. Res.*, *97*, 681–686.

Dugdale, R. C., C. O. Davis, and F. P. Wilkerson (1997), Assessment of new production at the upwelling center at Point Conception, California, using nitrate estimated from remotely sensed sea surface temperature, *J. Geophys. Res.*, *102*, 8573–8585.

Eppley, R. W., and B. J. Peterson (1979), Particulate organic matter flux and planktonic new production in the deep ocean, *Nature*, *282*, 677–680.

Fernández I., C. (2003), Cycle de l'azote et production primaire dans l'Atlantique Nord-Est: Suivi saisonnier et influence de la meso échelle, Ph.D. thesis, 331 pp., Univ. de la Méditerranée, Marseille, France.

Fernández I., C., P. Raimbault, G. Caniaux, N. Garcia, and P. Rimmelin (2005), Influence of mesoscale eddies on nitrate distribution during the POMME program in the north-east Atlantic Ocean, *J. Mar. Syst.*, *55*, 155–175.

Frazel, D. W., and G. Berberian (1990), Distributions of chlorophyll and primary productivity in relation to water column structure in the eastern North Atlantic Ocean, *Global Biogeochem. Cycles*, *4*, 241–251.

Gentilhomme, V., and P. Raimbault (1994), Absorption et régénération de l'azote dans a zone frontale du courant algérien (Méditerranée Occidentale): Réévaluation de la production nouvelle, *Oceanol. Acta*, *17*, 555–562.

Glibert, P. M., F. Lipschultz, J. J. McCarthy, and M. A. Altabet (1982), Isotope dilution models of uptake and remineralization of ammonium by marine plankton, *Limnol. Oceanogr.*, *27*, 639–650.

Gruber, N., and J. L. Sarmiento (1997), Global patterns of marine fixation and denitrification, *Global Biogeochem. Cycles*, *11*, 235–266.

Harrison, W. G., T. Platt, and M. R. Lewis (1987), *f*-ratio and its relationship to ambient nitrate concentration in coastal waters, *J. Plankton Res.*, *9*, 235–248.

Harrison, W. G., E. J. H. Head, E. P. W. Horne, B. Irwin, W. K. W. Li, A. R. Longhurst, M. Paranjape, and T. Platt (1993), The western North Atlantic Bloom Experiment, *Deep Sea Res., Part II*, *40*, 279–305.

Harrison, W. G., L. R. Harris, and B. D. Irwin (1996), The kinetic of nitrogen utilization in the oceanic mixed layer: Nitrate and ammonium interactions at nanomolar concentrations, *Limnol. Oceanogr.*, *41*, 16–32.

Henson, S. A., R. Sanders, J. T. Allen, I. S. Robinson, and L. Brown (2003), Seasonal constraints on the estimation of new production from space using temperature-nitrate relationships, *Geophys. Res. Lett.*, *30*(17), 1912, doi:10.1029/2003GL017982.

Koblentz-Mishke, O. I., V. V. Volkovinsky, and J. G. Kabanova (1970), Plankton primary production of the world ocean, in *Scientific Exploration of the South Pacific*, edited by W. Wooster, pp. 183–193, Natl. Academy of Sci., Washington, D. C.

Le Cann, B., M. Assenbaum, J.-C. Gascard, and G. Reverdin (2005), Observed mean and mesoscale upper ocean circulation in the midlatitude northeast Atlantic, *J. Geophys. Res.*, doi:10.1029/2004JC002768, in press.

Lipschultz, F., N. R. Bates, C. Carlson, and D. A. Hansell (2002), New production in the Sargasso Sea: History and current status, *Global Biogeochem. Cycles*, *16*(1), 1001, doi:10.1029/2000GB001319.

Lochte, K., H. W. Ducklow, M. J. R. Fasham, and C. Stienens (1993), Plankton succession and carbon cycling at 47°N 20°W during the Join Global Ocean Flux Study North Atlantic Bloom Experiment, *Deep Sea Res.*, *40*, 91–114.

Longhurst, A. L., S. Sathyendranath, T. Platt, and C. Caverdhill (1995), An estimate of global primary production in the ocean from satellite radiometer data, *J. Plankton Res.*, *17*, 1245–1271.

Louanchi, F., and R. G. Najjar (2001), Annual cycles of nutrients and oxygen in the upper layers of the North Atlantic Ocean, *Deep Sea Res., Part II*, *48*, 2155–2171.

Maixandeau, A., et al. (2005), Microbial community production, respiration, and structure of the mircrobial food web of an ecosystem in the northeastern Atlantic Ocean, *J. Geophys. Res.*, doi:10.1029/2004JC002694, in press.

Martin, J. H., S. E. Fitzwater, R. M. Gordon, C. N. Hunter, and S. J. Tanner (1993), Iron, primary production and carbon flux studies during the JGOFS North Atlantic Bloom Experiment, *Deep Sea Res., Part II*, *40*, 115–134.

McGillicuddy, D. J., Jr., R. Johnson, D. A. Siegel, A. F. Michaels, N. R. Bates, and A. H. Knap (1999), Mesoscale variations of biogeochemical properties in the Sargasso Sea, *J. Geophys. Res.*, *104*, 13,381–13,394.

Mémery, L., G. Reverdin, J. Paillet, and A. Oschlies (2005), Introduction to the POMME special section: Thermocline ventilation and biogeochemical tracer distribution in the northeast Atlantic Ocean and impact of mesoscale dynamics, *J. Geophys. Res.*, doi:10.1029/2005JC002976, in press.

Morel, A., and J. M. André (1991), Pigment distribution and primary production in the western Mediterranean as derived and modeled from coastal zone color scanner observations, *J. Geophys. Res.*, *96*, 12,685–12,698.

Morel, A., and S. Maritorena (2001), Bio-optical properties of oceanic waters: A reappraisal, *J. Geophys. Res.*, *106*, 7163–7180.

Morin, P., M. V. M. Wafar, and P. Le Corre (1993), Estimation of nitrate flux in a tidal front from satellite-derived temperature data, *J. Geophys. Res.*, *98*, 4689–4695.

Murray, J. M., J. N. Downs, S. Strom, C.-L. Wei, and H. W. Jannasch (1989), Nutrient assimilation, export production and ^{234}Th scavenging in the eastern equatorial Pacific, *Deep Sea Res., Part A*, *36*, 1471–1489.

Nixon, S. W. (1995), Coastal eutrophication: A definition, social causes and future concerns, *Ophelia*, *41*, 199–220.

Paillet, J., and M. Arhan (1996), Shallow pycnoclines and mode water subduction in the eastern North Atlantic, *J. Phys. Oceanogr.*, *26*, 96–114.

Pingree, R. D., and B. Le Cann (1992), Three anticyclonic Slope Water Oceanic eDDIES (SWODDIES) in the Southern Bay of Biscay in 1990, *Deep Sea Res., Part A*, *39*, 1147–1175.

Platt, T., and W. G. Harrison (1985), Biogenic fluxes of carbon and oxygen in the ocean, *Nature*, *318*, 55–58.

Priscu, J. C., and M. T. Downes (1985), Nitrogen uptake, ammonium oxidation and nitrous oxide (N_2O) levels in the coastal waters of western Cook Strait, New Zealand, *Estuarine Coast. Shelf Sci.*, *20*, 529–542.

Raimbault, P., G. Slawyk, B. Boudjellal, C. Coatanoan, P. Conan, B. Coste, N. Garcia, T. Moutin, and M. Pujo-Pay (1999), Carbon and nitrogen uptake and export in the equatorial pacific at 150°W: Evidence of an efficient regenerated production cycle, *J. Geophys. Res.*, *104*, 3341–3356.

Reverdin, G., M. Assenbaum, and L. Prieur (2005), Eastern North Atlantic Mode Waters during POMME (September 2000–2001), *J. Geophys. Res.*, doi:10.1029/2004JC002613, in press.

Rios, A. F., F. F. Pérez, and F. Fraga (1992), Water masses in the upper and middle North Atlantic Ocean east of the Azores, *Deep Sea Res., Part A*, *39*, 645–658.

Sathyendranath, S., T. Platt, E. P. W. Home, W. G. Harrison, O. Ulloa, R. Outerbridge, and N. Hoepffner (1991), Estimations of new production in the ocean by compound remote-sensing, *Nature*, *353*, 129–133.

Siegel, D. A., R. R. Iturriaga, R. C. Smith, H. Pak, T. D. Dickey, J. Marra, and S. Barker (1990), Meridional variations of the springtime phytoplankton community in the Sargasso Sea, *J. Mar. Res.*, *48*, 379–412.

Slawyk, G., and Y. Collos (1984), ^{13}C and ^{15}N uptake by marine phytoplankton III. Interactions in euphotic zone profiles of stratified oceanic areas, *Mar. Ecol. Prog. Ser.*, *19*, 223–231.

Slawyk, G., and P. Raimbault (1995), Simple procedure for the simultaneous recovery of dissolved inorganic and organic nitrogen in ^{15}N-tracer experiments and improving the isotopic mass balance, *Mar. Ecol. Prog. Ser.*, *124*, 289–299.

Slawyk, G., Y. Collos, and J. C. Auclair (1977), The use of the ^{13}C and ^{15}N isotopes for the simultaneous measurement of carbon and nitrogen turnover rates, *Limnol. Oceanogr.*, *22*, 925–932.

Slawyk, G., M. Minas, Y. Collos, L. Legendre, and S. Roy (1984), Comparison of radioactive and stable isotope tracer techniques for measuring photosynthesis: ^{13}C and ^{14}C uptake by marine phytoplankton, *J. Plankton Res.*, *6*, 249–257.

Takahashi, T., T. T. Takahashi, and S. C. Sutherland (1995), An assessment of the role of the North Atlantic as a CO_2 sink, *Philos. Trans. R. Soc. London, Ser. B*, *348*, 143–152.

Takahashi, T., R. A. Feely, R. Weiss, R. H. Wanninkhof, D. W. Chipman, S. C. Sutherland, and T. T. Takahashi (1997), Global air-sea flux of CO_2: An estimate based on measurements of sea-air pCO_2 differences, *Proc. Natl. Acad. Sci.*, *94*, 8292–8299.

Takahashi, T., R. H. Wanninkhof, R. A. Feely, R. F. Weiss, D. W. Chipman, N. Bates, J. Olafsson, C. Sabine, and C. S. Sutherland (1999), Net sea-air CO_2 flux over the global oceans: An improved estimate based on the sea-air pCO_2 difference, in *Proceedings of the Second International Symposium, CO_2 in the Oceans*, pp. 9–14, Cent. for Global Environ. Res., Natl. Inst. for Environ. Stud., Tsukuba, Japan.

Takahashi, T., et al. (2002), Global sea-air CO_2 flux based on climatological surface ocean pCO_2 and seasonal biological and temperature effects, *Deep Sea Res., Part II*, *49*, 1601–1622.

Thyssen, M., D. Lefèvre, G. Caniaux, J. Ras, L. Dugrais, C. Fernández I., and M. Denis (2005), Spatial distribution of heterotrophic bacteria in the northeast Atlantic (POMME study area in spring 2001), *J. Geophys. Res.*, doi:10.1029/2004JC002670, in press.

Ward, B. B., K. A. Kilpatrick, E. Renger, and R. W. Eppley (1989), Biological cycling in the nitracline, *Limnol. Oceanogr.*, *34*, 493–513.

Wirtky, K. (1981), An estimate of equatorial upwelling in the Pacific, *J. Phys. Oceanogr.*, *11*, 1205–1214.

Zehr, J. P., and B. B. Ward (2002), Nitrogen cycling in the ocean: New perspectives on processes and paradigms, *Appl. Environ. Microbiol.*, *68*, 1015–1024.

G. Caniaux, National de Recherche Météorologique, 42 Av. de Coriolis, F-31057 Toulouse, France. (guy.caniaux@meteo.fr)

C. Fernández I., N. Garcia, P. Raimbault, and P. Rimmelin, Laboratoire d'Océanographie et de Biogéochimie, UMR 6535, Centre National de Recherche Scientifique, Centre d'Océanologie de Marseille, Université de la Méditerranée, Campus de Luminy, F-13288 Marseille Cedex 09, France. (fernandez@com.univ-mrs.fr; garcia@com.univ-mrs.fr; raimbaul@com.univ-mrs.fr; rimmelin@com.univ-mrs.fr)